Pressure-induced transitions in solid nitrogen: Role of dispersive interactions.

Beyond a single-determinantal description of the density matrix of periodic systems: Experimental versus theoretical Compton profiles of crystalline silicon

A. Erba,[1,*] M. Itou,[2] Y. Sakurai,[2] R. Yamaki,[3] M. Ito,[3] S. Casassa,[1] L. Maschio,[1] A. Terentjevs,[1,†] and C. Pisani[1]

[1]*Dipartimento di Chimica IFM and Centre of Excellence NIS (Nanostructured Interfaces and Surfaces), Università di Torino, via P. Giuria 5, I-10125 Torino, Italy.*

[2]*Japan Synchrotron Radiation Research Institute, SPring-8 1-1-1 Kouto, Sayo, Hyogo 679-5198, Japan*

[3]*Graduate School of Engineering, Gunma University, 1-5-1 Tenjin-cho, Kiryu, Gunma 376-8515, Japan*

(Received 17 November 2010; revised manuscript received 13 January 2011; published 28 March 2011)

Compton profiles of crystalline silicon with a high statistical accuracy and high-resolution (0.11 a.u. in full width at half-maximum) are measured along the three main crystallographic directions and are compared to the predictions of *ab initio* simulations performed at different levels of theory, within and beyond one-electron approximations. The analysis of the Fourier transform of the Compton profiles reveals the failure of the density matrix extracted from single-determinantal models in reproducing some fine features of the electron momentum density of crystalline materials that can be attributed to the instantaneous Coulomb correlation of the electronic motions. The use of a post–Hartree-Fock periodic scheme allows such features to be satisfactorily reproduced.

DOI: 10.1103/PhysRevB.83.125208 PACS number(s): 78.70.−g, 31.15.A−, 61.66.Bi, 71.15.Dx

I. INTRODUCTION

The simulation of crystalline systems is nowadays standard practice in the frame of one-electron *ab initio* approximations: Hartree-Fock (HF), Kohn-Sham density-functional-theory (KS-DFT), and mixed (hybrid-exchange) schemes. Once the corresponding Hamiltonian has been chosen, the computation can be carried out with a very high numerical accuracy. To check the quality and the limitations of the solutions so provided, we have recently advocated more extensive use of the one-electron density matrix (DM) as a subtler probe than just the total energy E;[1] in fact, a number of DM-related properties, such as the electron charge density (ECD) $\rho(\mathbf{r})$ and the electron momentum density (EMD) $\pi(\mathbf{p})$ are susceptible to detailed comparison with the experiment. It is known, in particular, that the most popular among the one-electron approximations, namely, KS-DFT, is conceived and calibrated in such a way as to describe a set of independent pseudoparticles that reproduce, in principle, the *exact* ECD of the ground state of the system. Precisely due to this constraint, one cannot expect that the same set of occupied KS orbitals can provide its EMD satisfactorily as well.[2] Ragot has recently presented a detailed analysis of this topic,[3] and shown that current KS-DFT schemes perform in fact worse than HF when EMD-related quantities are considered. Similar conclusions were reached by Hart and Thakkar, who compared the performance of different theoretical schemes (HF, post-HF, and DFT) in reproducing the EMD moments of a set of 68 closed-shell molecules:[4] generally speaking, HF was shown to perform better in this respect than DFT.

From an experimental point of view, Compton scattering experiments constitute a very powerful tool for the reconstruction of the EMD of crystalline systems; this technique is finding renewed interest in the solid state community, mainly due to the enhancement of the resolution of its outcomes (Compton profiles; CPs), made possible from the availability of synchrotron radiation.[5,6] In recent years, this technique has been applied to the study of many "disordered" systems;[7–11] nevertheless, its main field of application still remains that of crystalline compounds, whose intrinsic anisotropy constitutes a source of additional information.[12–17]

The importance of comparing accurate experimental and theoretical EMDs is clear from the above: this is precisely the aim of this study, which concerns the prototypical case of crystalline silicon. It is motivated by two elements of novelty in the respective areas. On the one hand, directional CPs of unprecedented accuracy have been measured using an intense synchrotron radiation source. On the other hand, we are now in a position to calculate EMDs of crystalline systems using not only a variety of one-electron approximations, but also a post-HF technique that includes explicitly the Coulomb instantaneous correlation between electrons. A preliminary report on this subject has recently been published;[18] we provide here a more complete account of the experimental results and of the theoretical schemes adopted.

Our CRYSCOR code[19–22] implements Møller-Plesset perturbation theory truncated at order 2 (MP2) in a *local*,[23] fully periodic formulation; its range of applicability is limited for the time being to the ground state of nonconducting crystals. The HF reference solution is provided by the CRYSTAL program.[24] In recent years, CRYSCOR has been applied to the study of correlation effects on the energetic properties of many typologies of crystals like rare gases,[25–27] ice,[28–30] molecular crystals,[31–33] TiO_2,[34] and adsorption of atoms and molecules on ionic and covalent surfaces.[35,36] In a few cases, the effect of the MP2 correction on DM-related properties has been investigated.[1,37]

The history of experimental determinations of silicon CPs has been long and fruitful. Since the first experimental work, based on positron-annihilation measurements,[38] through the γ-ray study by Reed and Eisenberger,[39] which, for many years, was the benchmark in this field, through the work of Pattison *et al.*,[40] Shiotani *et al.*,[41] and Kubo *et al.*,[42] up to the present data, the experimental resolution has progressively improved, resulting in enhancement of the CP anisotropies.

A lot of theoretical work has been carried out to reproduce such data. The positron-annihilation results[38] were qualitatively reproduced in a pioneering model-potential study by

Stroud and Ehrenreich.[43] The results obtained by Seth and Ellis[44] with a Hartree-Fock-Slater variational method appear to be in reasonable agreement with the results of Reed and Eisenberger,[39] except for an overestimation by about 1.5% in the region of small p values. The inversion procedure devised by Mueller[45] for reconstruction of the EMD from the same experimental CPs proved to be reliable. The pseudopotential calculations performed by Nara *et al.*[46] with different model potentials correctly reproduced the oscillations of the CP anisotropies but largely overestimated their amplitudes, thus leading to the conclusion that these observables are insensitive to the adopted model potential: this conclusion is questionable, however, due to the different scale of computed and experimental results, as commented on in Sec. V. Special reference can be made to the work by Pisani *et al.*,[47] reporting very accurate simulations of the CPs of crystalline silicon at the HF level performed with the CRYSTAL program (the one used here to perform HF and DFT calculations), compared to the experimental results of Pattison *et al.*[40] The calibration of the computational parameters implied in these calculations and the role of the adopted basis set were accurately analyzed and represent the starting point for the assessment of the present computational setup (see Sec. III). In an attempt to go beyond one-electron approximation, an *ab initio* variational quantum Monte Carlo study was performed by Králik *et al.*[48] where the effect of electron correlation was investigated; the authors concluded that, when electron correlation is explicitly considered, the computed profiles are lowered by about 1% near $p = 0$, thus reducing the discrepancy with the experiment in this region, which, however, still remains evident.

The structure of this paper is as follows. Section II reports the experimental setup and the description of the data processing adopted to correct the measured CPs for absorption, detection efficiency, and multiple scattering. Section III presents the computational framework. The adopted setup is described, with special attention given to the choice of the basis set of localized Gaussian functions, which is calibrated with respect to a well-converged plane-wave basis set. The different modes of description of the EMD are defined in Sec. IV: their main features are illustrated, and the relations among them introduced. In Sec. V we present and discuss our results. The quality of our computational setup is first analyzed by checking the accuracy of the computed values of x-ray structure factors. The experimental and theoretical description of the EMD are next compared, with reference to CPs and to their one-dimensional Fourier transform, the autocorrelation function (AF). A general discussion follows. Some conclusions are drawn in Sec. VI.

II. EXPERIMENTAL INFORMATION

Single crystals of silicon with surface normal oriented along the [100], [110], and [111] directions were used. The size of the crystals was $10 \times 10 \times 0.5$ mm. The experiment was carried out at 300 K. CPs were measured at the BL08W beamline of SPring-8, where incident x-ray beams of 115.5 keV are available with a photon flux of 1×1013 photons/s at the sample. The scattering angle was 165.3°. The high-resolution spectrometer for Compton-scattered x rays consists of a triangular Cauchois-type Ge (620) crystal bent to a radius of 3200 mm and an x-ray image intensifier as a position sensitive detector.[49,50] The overall instrumental resolution was 0.11 a.u. in full width at half-maximum (FWHM). The accumulated count at the Compton peak channel was about 2×105 counts/0.025 a.u. for each profile. The measured profiles were duly corrected for absorption, detection efficiency, and scattering cross section. Areas under the corrected profiles were normalized to the effective total number of electrons, and the normalized profiles are used as total CPs. For evaluating the contribution of multiple scattering, we measured a 5-mm-thick Si single crystal with the surface normal along the [100] direction, where the multiple scattering is stronger than that of the 0.5-mm-thick sample. With the ratio of the total intensity of multiple scattering to that of single scattering obtained by a Monte Carlo simulation,[51] the contribution of multiple scattering was estimated from the experimental profiles of the 0.5- and 5-mm-thick samples. The ratio of the total intensity of multiple scattering to that of single scattering was 1.7% for 0.5-mm-thick samples. Systematic errors, mostly coming from the estimate of the multiple scattering contribution, are canceled out in the CP anisotropies since both the dimensions and the orientation of the sample plates are the same for all three CP measurements. The statistical error at $p = 0$ is approximately 0.2% the value of the total CP.

III. COMPUTATIONAL TECHNIQUES

All simulations described below are performed using two "periodic" *ab initio* codes: CRYSTAL[24] and CRYSCOR.[19–22] All quantities of interest in both programs are expressed as linear combinations of Gaussian "primitives" centered in high-symmetry positions: these functions are referred to in the following as atomic orbitals (AOs). The use of such a basis set (BS) is mandatory for the local correlation approach adopted in CRYSCOR. The experimental equilibrium geometry at 300 K ($a = 5.43$ Å) has been adopted for all calculations to maximize the comparability of the computed to the experimental data.

A. Computational setup

The CRYSTAL program is used here to perform both HF and DFT calculations. Four one-electron Hamiltonians are considered: the classical HF, two typical DFTs [a local density approximation (LDA)[52] and the generalized-gradient PBE[53]], and a hybrid DFT (B3LYP).[54] Accurate calibration of the basis set is perhaps the most delicate step in defining the optimal computational setup and is discussed in detail in Sec. III B, but it is not the only one. In CRYSTAL, the truncation of infinite lattice sums is controlled by five thresholds, T1 to T5, which are set here to 16, 12, 12, 15, 30. Note, in particular, that a tight value T1 = 16 must be adopted for a reliable description of CPs and related quantities, instead of the default value of 6, which is adequate for most other purposes: this is necessary to generate geometrical information on a sufficiently large set of lattice vectors. The DFT exchange-correlation contribution is evaluated by numerical integration over the cell volume: radial and angular points of the atomic grid are generated through Gauss-Legendre and Lebedev quadrature schemes, using a (75,974)p grid; grid pruning is adopted. Reciprocal space is sampled according to a regular sublattice with a shrinking

factor equal to 8, corresponding to 29 **k** points in the irreducible Brillouin zone.

After completing the self-consistent calculation, CRYSTAL determines via a unitary transformation of the manifold of occupied canonical crystalline orbitals (CO), $\{\psi_{j,\kappa}(\mathbf{r})\}$, the equivalent set of Wannier functions (WFs),[55–57] $\{w_{i,\mathbf{g}}(\mathbf{r})\}$. Here the indices i,j run from 1 to $N_0/2$, N_0 being the number of electrons per unit cell, while κ and **g** indicate the wave vector and the general direct lattice vector, respectively. WFs are real, well-localized, symmetry-adapted, mutually orthonormal $[\langle\, w_{i,\mathbf{g}} \,|\, w_{j,\mathbf{l}} \,\rangle = \delta_{ij}\,\delta_{\mathbf{gl}}]$, translationally equivalent $[w_{i,\mathbf{g}}(\mathbf{r}) = w_{i,\mathbf{0}}(\mathbf{r}-\mathbf{g})]$ functions.

WFs play an essential role in CRYSCOR, together with the complementary set of projected atomic orbitals (PAOs); the latter are local functions that span the virtual HF manifold and are obtained by projecting out of each AO its "occupied" portion.[23] The functions in the two sets are concisely indicated as $i,j,\ldots$ and $a,b,\ldots$, respectively. The MP2 energy $E^{(2)}$ can be written as a sum of all contributions E_{ij}^{ab}, each corresponding to a two-electron excitation from a pair of WFs to a pair of PAOs $[(ij)\uparrow\uparrow(ab)]$; the related amplitudes are calculated via a self-consistent procedure. Exploitation of translational symmetry allows us to impose the first WF (i) to belong to the reference zero cell.

The input parameters of CRYSCOR serve essentially to fix three kinds of tolerances, all concerning the treatment of WFs and PAOs. The first parameter simply determines the truncation of their tails: in the linear combinations that define WFs and PAOs, those AOs are disregarded whose coefficients are lower than t^c, here set to 0.0001. The other two parameters are used to exploit the local-correlation ansatz,[23,58] according to which all excitations can be ignored except those involving close-by WF and PAO pairs. More precisely, the following selection criteria are adopted. To the general WF (i) a *domain* $\mathcal{D}_i$ is associated consisting of a certain number of atoms close to it; here $\mathcal{D}_i$ is taken to correspond to the eight silicon atoms which constitute the first two stars of neighbors of a given covalent bond described by the i WF. Two WFs then define a *pair-domain* $\mathcal{D}_{(ij)}$ which is simply the union of the corresponding domains. Only those $[(ij)\uparrow\uparrow(ab)]$ excitations are retained for which, first, both PAOs, a and b, belong to atoms in $\mathcal{D}_{(ij)}$, and second, the distance d_{ij} between the centers of the two WFs is within a certain value D; in the present application, $D = 12$ Å. Once the relevant WF-PAO pairs are selected, the main computational step is the evaluation of the two-electron repulsion integrals, $(ia \mid jb)$, between the respective product distributions. The analytical calculation of such integrals is a very demanding task; a way out of this difficulty has been to estimate the electron repulsion intervals using a periodic variant of molecular density-fitting techniques,[21,59] with extraordinary savings in computer time and negligible loss of accuracy. Furthermore, if the two WFs are sufficiently far apart (say, beyond a certain distance D', here set to 8 Å), the electron repulsion intervals are evaluated at near-zero cost via a multipolar technique.

B. The basis set

The AOs $\chi_{\mu\mathbf{g}}(\mathbf{r})$ used as a BS by CRYSTAL and CRYSCOR are local, real functions of **r**, labeled by an index $\mu = 1,\ldots p$, which identifies their shape and location within the reference zero cell, and by an index **g**, which specifies the crystalline cell to which they belong. As is standard practice in molecular quantum chemistry, the AOs here are contractions of Gaussian "primitives" of angular momentum components ℓ, m centered in an atomic nucleus or at some special position in the cell.

The choice of a suitable AO-BS, as a compromise among the often conflicting requirements of accuracy, feasibility, and computational cost, is an important issue. In a recent study concerning the *ab initio* simulation of the DM of crystalline solids,[60] we have revised this problem by analyzing the performance of different AO-BSs in the reproduction of two quantities related to the ECD of silicon: the value of $\rho(\mathbf{r})$ at the bond midpoint and the F_{222} structure factor (whose nonzero value is a measure of the asphericity of the ECD about the individual atoms). For comparison, calculations were performed with the Quantum-ESPRESSO code,[61] where a plane-wave BS was used for the valence electrons, while the core contribution was described with the PAW (projector augmented waves) technique. In both cases the PBE Hamiltonian was adopted. The results of this comparison can be summarized as follows. (i) The plane-wave basis sets perform very well; with the improvement of their quality (represented by a unique parameter, the so-called *energy cutoff*), they rapidly converge to a definite value that can be taken as a reference. (ii) Improving the quality of the AO-BS implies providing a progressively better description of core electrons and allowing wider variational freedom for the valence electrons; along the series, the convergence to the reference value is slower and less uniform with respect to plane waves, but is finally achieved. (iii) The "converged" PBE results reproduce very accurately the experimental ECD data, as commented on in Sec. V A.

In the present work, we adopt the "best" AO-BS among those tried in that study, that is, the one labeled 8-41G***(sp); it represents an improved version of the 8-41G basis set explicitly reported in Ref. 47. The 10 core electrons with principal quantum numbers 1 and 2 are described by one s and one sp shell, respectively, both comprising an optimized combination of eight primitives. The rest of the BS provides ample variational freedom for the valence electrons. Apart from two independent sp shells of four and one primitive, respectively, we have three single-primitive *polarization* functions, two of d and one of f type. All these AOs are centered in the Si nuclei. In addition, the BS includes an sp-type shell (with exponent 1.4 a.u.) located at the midpoint of the Si-Si bond: this further shell was found to contribute to the proper description of the ECD at the center of the bond.

With this AO-BS, the HF CRYSTAL calculation provides an atomization energy of 0.235 E_h per unit cell of silicon (with reference to the HF limit for the atom), which is close to the estimated HF limit ($0.240 \pm 0.015 E_h$).[47] The MP2 energy evaluated with CRYSCOR is 0.100 E_h per cell, that is, the near totality of the correlation energy of crystalline silicon, estimated at $0.105 \pm 0.015 E_h$:[47] this shows that the present BS can provide sufficient flexibility for the description of low-lying excited states, as it is needed for the MP2 estimate of correlation effects.

IV. DENSITY MATRIX MANIPULATION

The spin-free DM of a crystalline, nonconducting, closed-shell system described by a one-electron Hamiltonian (X) can be written in several equivalent ways:

$$R^X(\mathbf{r};\mathbf{r}') = 2\sum_{j=1}^{N_0/2}\sum_{\kappa}\psi^X_{j,\kappa}(\mathbf{r})\left[\psi^X_{j,\kappa}(\mathbf{r}')\right]^* \quad (1)$$

$$= 2\sum_{i=1}^{N_0/2}\sum_{\mathbf{g}} w^X_{i,\mathbf{g}}(\mathbf{r})\; w^X_{i,\mathbf{g}}(\mathbf{r}') \quad (2)$$

$$= \sum_{\mathbf{g},\mathbf{l}}\sum_{\mu\nu} P^X_{\mu\nu\mathbf{g}}\;\chi_{\mu\mathbf{l}}(\mathbf{r})\;\chi_{\nu(\mathbf{l}+\mathbf{g})}(\mathbf{r}'). \quad (3)$$

In the first line, it is given in terms of the COs; in the second, of the WFs; and in the third, of the AOs. The elements of the $\mathbf{P}^X$ matrix that appear in the last expression are defined as follows per each pair of AOs μ and ν in two arbitrary cells related to each other by a lattice vector $\mathbf{g}$:

$$P^X_{\mu\nu\mathbf{g}} = 2\sum_{j=1}^{N_0/2}\sum_{\kappa} e^{-\imath\,\kappa\cdot\mathbf{g}}\left[a^X_{j,\kappa;\mu}\left(a^X_{j,\kappa;\nu}\right)^*\right], \quad (4)$$

where $a^X_{j,\kappa;\mu}$ denote the coefficients of the COs in the AO-BS (translational invariance is exploited here).

Since the early days of quantum chemistry, it has been known that one of the main deficiencies of single-determinantal approximations is their inability to describe the *Coulomb hole*, that is, the fact that electrons with opposite spin instantaneously correlate their motions so as to stay as far apart from each other as possible. A way to eliminate this inadequacy, which affects not only the energy of the system, but also its DM, may consist either in the explicit inclusion in the expression of the wave function of terms that depend on the interelectronic distance,[62] or in a multideterminantal expansion, or in a combination of the two schemes.[63]

These techniques are not easily applied to "large" systems, in particular, to periodic ones. To extract information on the DM from a nonvariational perturbative approach such as the MP2 one implemented in CRYSCOR, rather than referring to the wave function, it is preferable to adopt a Lagrangian approach,[64] according to which the DM provides the first-order response of the energy of the system to an arbitrary external one-electron perturbation. Note that even if formulations (3) and (4) of the DM are no longer usable when one goes beyond the one-electron approximation, we can still exactly write within the selected representative Fock space,

$$R(\mathbf{r};\mathbf{r}') = \sum_{\mathbf{g},\mathbf{l}}\sum_{\mu\nu} P_{\mu\nu\mathbf{g}}\;\chi_{\mu\mathbf{l}}(\mathbf{r})\;\chi_{\nu(\mathbf{l}+\mathbf{g})}(\mathbf{r}'), \quad (5)$$

with an appropriately corrected $\mathbf{P}$ matrix.

CRYSCOR provides precisely a Lagrangian estimate of the correction $\mathbf{P}^{\mathrm{MP2}}$ to be applied to the HF-DM:[1,65]

$$\mathbf{P}^{\mathrm{HF+MP2}} = \mathbf{P}^{\mathrm{HF}} + \mathbf{P}^{\mathrm{MP2}}. \quad (6)$$

Once an estimate of the DM in the coordinate representation $R(\mathbf{r};\mathbf{r}')$ is available, its expression in the momentum representation $P(\mathbf{p};\mathbf{p}')$ is obtained through a six-dimensional Fourier transform. We are interested here in its diagonal element, the EMD $\pi(\mathbf{p}) = P(\mathbf{p};\mathbf{p})$, and in three related functions, the AF, $B(\mathbf{r})$[66] (also referred to in the literature as the *internally folded density*),[67] the directional AF, $B_{hkl}(r)$, and the directional CP, $J_{hkl}(p)$. A number of useful relationships exist among these quantities and between them and the AO representation of the DM, Eq. (5).

The AF is equivalently defined as the 3D Fourier transform of the EMD, or as the auto-correlation integral of the position DM:

$$B(\mathbf{r}) = \int \pi(\mathbf{p})\, e^{\imath\,\mathbf{p}\cdot\mathbf{r}}\, d\mathbf{p} \equiv \frac{1}{L}\int R(\mathbf{r}';\mathbf{r}+\mathbf{r}')\, d\mathbf{r}', \quad (7)$$

the normalization factor $1/L$ ensuring that the condition is obeyed: $B(\mathbf{0}) = N_0$. From here and from Eq.n (5), a computationally convenient expression is obtained:

$$B(\mathbf{r}) = \sum_{\mu\nu}\sum_{\mathbf{g}} P_{\mu\nu\mathbf{g}}\; S_{\mu\nu\mathbf{g}}(\mathbf{r}), \quad (8)$$

with

$$S_{\mu\nu\mathbf{g}}(\mathbf{r}) = \int \chi_{\mu\mathbf{0}}(\mathbf{r}')\;\chi_{\nu\mathbf{g}}(\mathbf{r}+\mathbf{r}')\, d\mathbf{r}'. \quad (9)$$

For each $[hkl]$ crystallographic direction identified by the unit vector $\mathbf{e}_{hkl}$, two interrelated functions of a single variable can be defined, namely, the directional AF, $B_{hkl}(r) = B(r\,\mathbf{e}_{hkl})$, and the directional CP, $J_{hkl}(p)$:

$$J_{hkl}(p) = \int \pi(\mathbf{q})\;\delta(\mathbf{q}\cdot\mathbf{e}_{hkl} - p)\, d\,\mathbf{q} \quad (10)$$

$$= \frac{1}{2\pi}\int B_{hkl}(r)\; e^{-\imath\,p\,r}\, dr. \quad (11)$$

Within the sudden-impulse approximation, $J_{hkl}(p)$ is directly comparable to the outcome of Compton-scattering experiments,[68] after correcting the latter for limited resolution and multiple scattering effects. In particular, the effect of limited resolution can be expressed as a convolution of the "infinite resolution" data with a normalized Gaussian function $g(p;\sigma_{\mathrm{cp}})$ characterized by a given standard deviation σ_{cp} (or, equivalently, by the FWHM parameter $w_{\mathrm{cp}} = \sigma_{\mathrm{cp}}\cdot 2\sqrt{2\log 2}$), which quantifies the experimental resolution:

$$J^{\sigma}_{hkl}(p) = \int_{-\infty}^{+\infty} J_{hkl}(p')\; g(p-p';\,\sigma_{\mathrm{cp}})\, dp'$$

$$= \frac{1}{2\pi}\int_{-\infty}^{+\infty} B^{\sigma}_{hkl}(r)\;\; e^{-\imath\,p\,r}\, dr \quad (12)$$

In the last integrand a "finite-resolution AF" appears, which is simply the *product* of the AF from Eq. (7) or (8) by a Gaussian function $g(r,\sigma_{\mathrm{br}})$, with $\sigma_{\mathrm{br}} = 1/\sigma_{\mathrm{cp}}$, and can be extracted from the experimental CP simply by Fourier back-transformation.

As shown below, a lot of information can be obtained from the *anisotropies* of the AFs, $B_{hkl}(r) - B_{h'k'l'}(r)$, or of the CPs, $J_{hkl}(p) - J_{h'k'l'}(p)$, since many experimental errors are canceled out when performing these differences. A manipulation that will prove useful, though not rigorously justified, is the separation of the DM and related quantities into a *core* and a *valence* part. In many instances, as in the case of silicon, the *core bands* (those with $j = 1, N_c/2$) are energetically much lower than the other bands; their eigenvalues, and the corresponding eigenfunctions, are very

similar to those of the isolated atoms. This corresponds to the well-known chemical property that only *valence bands* (those with $N_c/2 < j \leqslant N_0/2$) are affected by the formation of the crystal. We can then identify a core DM $R^{X,\mathrm{core}}(\mathbf{r};\mathbf{r}')$ and a valence DM $R^{X,\mathrm{val}}(\mathbf{r};\mathbf{r}')$ by extending the sums over j in Eq. (4) to the two sets of bands, respectively: this is, in fact, the approach adopted in this work.

When going beyond the one-electron approximation we can still tentatively maintain the above separation. In particular, when calculating the MP2 correction to the DM, we are only considering biexcitations from valence WFs, that is, from WFs that span the valence bands altogether. Therefore, the matrix $\mathbf{P}^{\mathrm{MP2}}$ in Eq. (6) would be more properly labeled $\mathbf{P}^{\mathrm{MP2,val}}$. Since the EMD, the AF, and the directional AFs and CPs are linearly related to the DM, the core-valence separation can be applied to them as well.

Finally, an important feature of calculated AFs must be recalled. For an insulating crystal, simulated with a one-electron Hamiltonian X, the DM can be formulated in terms of WFs, owing to Eq. (2). By using this expression in Eq. (7), and taking into account the orthonormality of the WFs, the following *nodal property* is found to hold true:

$$B^X(\mathbf{g}) = 0 \quad \text{for all lattice vectors} \quad \mathbf{g} \neq \mathbf{0} \tag{13}$$

As a consequence, directional AFs must exhibit an oscillatory behavior. The above property applies to both the core and the valence part of the AF, since the two sets of WFs are independent. However, $B^{X,\mathrm{core}}(\mathbf{r})$ is so small at any $\mathbf{g} \neq \mathbf{0}$ that the oscillations about 0 are entirely due to the valence part. Equation (13) holds true also for the finite-resolution AF $B^{X,\sigma}(\mathbf{r}) = B^X(\mathbf{r}) \times g(\mathbf{r},\sigma_{\mathrm{br}})$ [see Eq. (12)]. It no longer needs to be satisfied when going beyond the one-electron approximation. Therefore, departures from this condition when considering experimental AFs may be indicative of correlation effects not accounted for by one-electron Hamiltonians.

V. RESULTS AND DISCUSSION

A. ECD simulation: A reminder

Before comparing experimental with theoretical EMDs, let us briefly discuss what happens with the ECD. Reference is made here to the data reported by Lu *et al.*[69] and resulting from a very accurate elaboration of experimental x-ray structure factors; though relatively old, that paper is still an unsurpassed reference in this respect. All the results presented here were obtained by adopting the 8-41G***(sp) BS and the computational setup described in Sec. III A. As anticipated in Sec. I, the DFT is expected to accurately reproduce ECDs; as a consequence, the adequacy of our computational setup (in particular, of the adopted basis set) can be checked by comparing the DFT estimates of ECD-related properties with their experimental counterparts.

Table I reports a set of 18 static x-ray structure factors (F_{hkl}), computed with different Hamiltonians and compared to the experiment. The quality of the agreement can be measured, as usual, by the corresponding agreement factor reported in the last line in the table:

$$R^X = \sum_{hkl} \frac{\left|F^X_{hkl} - F^{\mathrm{exp}}_{hkl}\right|}{F^{\mathrm{exp}}_{hkl}} \times 100. \tag{14}$$

TABLE I. Theoretical versus experimental static structure factors F_{hkl} of crystalline silicon. Agreement factors in the last line are defined in Eq. (14).

hkl	HF	HF + MP2	LDA	PBE	exp
111	10.770	10.760	10.740	10.740	10.728
220	8.645	8.650	8.655	8.650	8.656
311	7.995	8.002	8.023	8.023	8.020
222	0.235	0.222	0.162	0.167	0.191
400	7.455	7.460	7.445	7.450	7.449
331	7.283	7.278	7.222	7.232	7.247
422	6.735	6.735	6.695	6.705	6.716
333	6.429	6.428	6.403	6.412	6.427
511	6.461	6.460	6.430	6.438	6.438
440	6.070	6.070	6.030	6.040	6.046
444	4.988	4.987	4.964	4.970	4.979
551	4.823	4.822	4.799	4.805	4.807
642	4.562	4.561	4.541	4.546	4.555
800	4.194	4.193	4.176	4.181	4.176
660	3.876	3.876	3.860	3.865	3.866
555	3.764	3.764	3.751	3.755	3.760
844	3.152	3.152	3.141	3.144	3.135
880	2.541	2.541	2.534	2.536	2.533
R	0.32%	0.28%	0.20%	0.14%	

As expected, the generalized-gradient PBE Hamiltonian performs extremely well ($R^{\mathrm{PBE}} = 0.14\%$), while the LDA Hamiltonian is slightly worse ($R^{\mathrm{LDA}} = 0.20\%$). The HF results are definitely less satisfactory ($R^{\mathrm{HF}} = 0.32\%$); the MP2 correction significantly improves them ($R^{\mathrm{HF+MP2}} = 0.28\%$) but not to an extent to bring them to the same level of quality as the KS results.

Similar conclusions are reached when considering the calculated ECD along the bond, reported in Fig. 1. The reference value here is the "experimental" density at the bond midpoint $\rho(\delta)$ (also estimated by Lu *et al.*), which is accurately

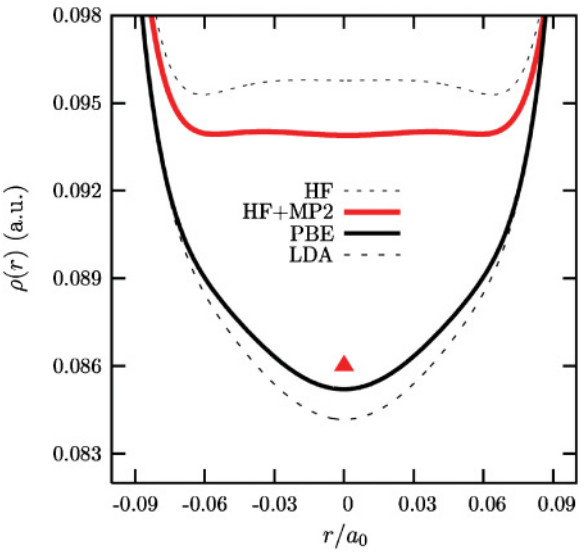

FIG. 1. (Color online) Calculated electron charge density along an Si-Si bond, near its midpoint. The experimental value at the midpoint is represented by the triangle.

predicted by the PBE Hamiltonian. The LDA slightly underestimates the value of $\rho(\delta)$, while HF strongly overestimates it; passing from HF to HF + MP2, the charge density at the bond midpoint decreases, but not by the full required amount.

B. CPs: Experiment versus theory

Table II reports the present experimental CP along [100] and the corresponding calculated one, both uncorrected, $J^{X}_{100}(p)$, and corrected, $J^{\sigma,X}_{100}(p)$, for the limited resolution of the spectrometer [see Eq. (12), with $\sigma = 0.047$ a.u.], for the cases $X =$ HF, HF + MP2, and PBE. It is shown that the effect of this correction is a reduction in the peak height of the computed infinite resolution CPs by about 0.1% near $p = 0$.

Figure 2 shows the corrected $J^{\sigma,X}_{100}(p)$ CPs, computed with the whole set of Hamiltonians used here (HF, HF + MP2, PBE, LDA, B3LYP), along with the experimental data, whose intrinsic uncertainty is about 0.2% at $p = 0$. At this level of detail, all the theoretical CPs coincide among themselves and are almost indistinguishable from the experimental curve, except in the vicinity of $p = 0$: there, the value of the experimental CP is less than that of the calculated ones by about 5%. This relevant feature has been reported also in previous papers: notable among them, the one by Kubo *et al.*,[42] who performed DFT calculations at various levels of sophistication to analyze their experimental CPs and the

TABLE II. Experimental versus calculated CPs of crystalline Si along [100]. For each Hamiltonian both the infinite-resolution [$J(\mathbf{p})$] and the finite-resolution [$J^{\sigma}(\mathbf{p})$] CPs are reported.

	Exp.	HF + MP2		HF		PBE	
p	$J^{\sigma}(\mathbf{p})$	$J^{\sigma}(\mathbf{p})$	$J(\mathbf{p})$	$J^{\sigma}(\mathbf{p})$	$J(\mathbf{p})$	$J^{\sigma}(\mathbf{p})$	$J(\mathbf{p})$
0.0	4.1093	4.2849	4.2891	4.3143	4.3187	4.3198	4.3237
0.1	4.0904	4.2637	4.2692	4.2925	4.2980	4.3004	4.3052
0.2	4.0252	4.1919	4.1993	4.2209	4.2282	4.2371	4.2435
0.3	3.9120	4.0554	4.0652	4.0849	4.0952	4.1146	4.1254
0.4	3.7206	3.8390	3.8512	3.8649	3.8778	3.9017	3.9167
0.5	3.4482	3.5352	3.5458	3.5523	3.5633	3.5813	3.5930
0.6	3.1007	3.1681	3.1747	3.1743	3.1811	3.1891	3.1957
0.7	2.7315	2.7802	2.7841	2.7759	2.7797	2.7781	2.7822
0.8	2.3666	2.4067	2.4075	2.3935	2.3941	2.3833	2.3838
0.9	2.0509	2.0789	2.0761	2.0596	2.0565	2.0405	2.0365
1.0	1.8076	1.8220	1.8179	1.8003	1.7959	1.7808	1.7755
1.1	1.6274	1.6390	1.6361	1.6182	1.6151	1.6052	1.6017
1.2	1.5056	1.5126	1.5114	1.4947	1.4933	1.4892	1.4880
1.3	1.4143	1.4215	1.4215	1.4071	1.4070	1.4068	1.4069
1.4	1.3463	1.3505	1.3512	1.3394	1.3400	1.3412	1.3421
1.5	1.2911	1.2903	1.2914	1.2820	1.2831	1.2841	1.2853
1.6	1.2310	1.2360	1.2373	1.2298	1.2311	1.2313	1.2326
1.7	1.1818	1.1849	1.1864	1.1804	1.1819	1.2313	1.1825
1.8	1.1340	1.1357	1.1373	1.1325	1.1341	1.1324	1.1341
1.9	1.0875	1.0875	1.0892	1.0852	1.0870	1.0847	1.0865
2.0	1.0430	1.0399	1.0417	1.0383	1.0401	1.0374	1.0392
2.5	0.8169	0.8169	0.8188	0.8166	0.8185	0.8139	0.8158
3.0	0.6296	0.6285	0.6303	0.6285	0.6303	0.6257	0.6275
3.5	0.4884	0.4816	0.4832	0.4816	0.4832	0.4793	0.4809
4.0	0.3754	0.3719	0.3733	0.3719	0.3733	0.3702	0.3716
5.0	0.2346	0.2333	0.2332	0.2333	0.2333	0.2324	0.2323

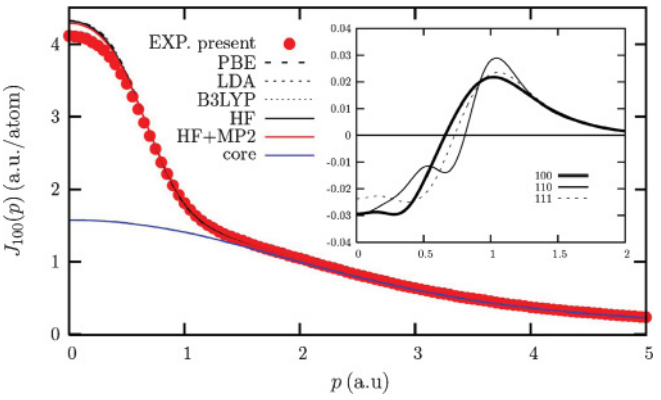

FIG. 2. (Color online) Experimental versus calculated CPs along [100]. The momentum **p** is in atomic units; J, in atomic units per atom. All theoretical results are convoluted with the experimental resolution function. Inset: MP2 contribution to the HF + MP2 CPs.

variational quantum Monte Carlo study by Králik *et al.*[48] Possible reasons for this discrepancy are discussed in Sec. V D. The Hamiltonian that provides the best description of the CPs near $p = 0$ is HF + MP2. The MP2 correction to the HF reference CPs is reported in the inset in Fig. 2 for the three main crystallographic directions. It is shown that when the instantaneous correlation between the electronic motions is explicitly accounted for, the CPs are decreased at low momenta and increased near $p = 1$ a.u. Even if small (the MP2 correction is always within 1% of the total), this correction brings the computed profiles closer to their experimental counterpart. This result is expected since the main effect of the correlation of electron motions is allowing them to stay closer to the nuclei, hence to increase, on average, their kinetic energy. Note, however, that in the present scheme the MP2 correction is applied only to valence electrons. An estimate of the corresponding effect on core electrons brings in a further reduction of about 1% of the theoretical CPs near $p = 0$. Relativistic effects on the description of core electrons are not investigated.

Due to the fact that the core EMD is essentially isotropic, the consequences of an inadequate description of the corresponding distribution should cancel out when considering CP anisotropies. Figure 3 compares experimental with calculated data for these quantities, which convey a lot of information since they reflect the intrinsic anisotropy of the electronic structure of the crystal. We also report there, for the sake of reference, some older experimental data of Pattison *et al.*[40] Since the resolution for that experiment was different (and worse) with respect to the present one, which was used for correcting the calculated CPs, those data are not strictly comparable to the computed ones. It is worth noting that, with that poorer resolution, it was almost impossible to assess the quality of the agreement achieved with the different Hamiltonians; this was, indeed, the conclusion reached by Nara *et al.*[46] By virtue of the extremely high resolution of the present CPs, the anisotropy of the EMD is revealed in extreme detail, in strict connection with the resolution of the spectrometer: while passing from $w_{cp} = 0.41$ in the work by Pattison *et al.*[40] to $w_{cp} = 0.11$ in the present data, the amplitudes of the oscillations of the experimental CP anisotropies increase by

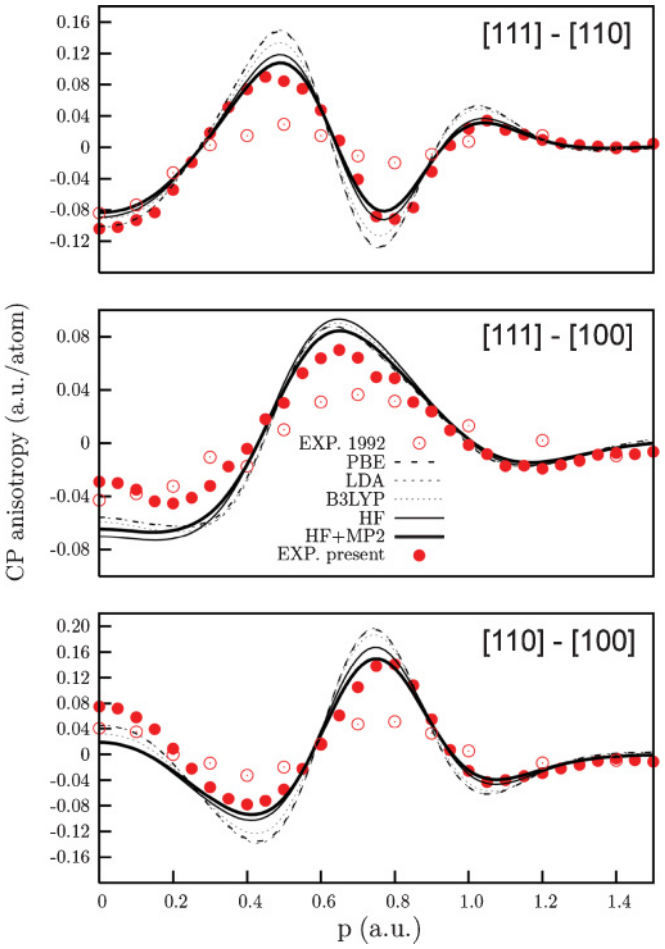

FIG. 3. (Color online) CP anisotropies among the three main crystallographic directions of silicon as computed with several Hamiltonians and compared to the new experiment. Some older (1992) data of Pattison *et al.*[40] are also reported.

about a factor of 2. This allows us to discriminate the various theoretical schemes, even if the agreement with the experiment is generally good for all of them. At variance with the case of the ECD (see Sec. V A), HF and, especially, HF + MP2 appear to perform much better than DFT-based treatments in reproducing the finest features of the CP anisotropies: this is not a surprise, for the reasons cited in Sec. I. The PBE and LDA Hamiltonians are found to exaggerate the anisotropies by about the same amount, while HF significantly reduces them; the B3LYP hybrid Hamiltonian, as expected, provides an intermediate description. The effect of the explicit treatment of instantaneous electron correlation, as evaluated at the HF + MP2 level, is to reduce the anisotropies and to improve the agreement with the experiment.

C. AFs: Experiment versus theory

By means of Eq. (8) it is possible to obtain directly the calculated AFs and, if needed, to separate core and valence contributions. Their experimental counterpart is obtained in principle through a 1D Fourier transform of the corresponding CPs, which requires, however, knowledge of them up to $p = \infty$. Due to the finite range (0–10 a.u.) of the experimental CPs, the following computational scheme was applied to extract from them their valence part. The isotropic $J^{\mathrm{HF,core}}(p)$ has first been evaluated from the DM corresponding to the core bands of the HF periodic solution (see the "core" curve in Fig. 2). This contribution (duly convoluted for limited resolution) has been subtracted from all directional CPs; it has been verified that the use of other one-electron Hamiltonians resulted in no appreciable changes in the resulting valence CPs. The "experimental valence CPs" so obtained were practically 0 beyond 6 a.u., as expected. However, oscillations about 0 within the experimental error were left at high momenta. This numerical noise had to be eliminated because it would have been unduly amplified in performing the Fourier transform. In the region $1.6 < p < 10$ a.u., the valence data were therefore fitted with an exponential function. The directional experimental valence AFs were hence obtained by using the original pseudovalence CP data between 0 and 1.6 a.u., and the fitted ones beyond 1.6 a.u.

Figure 4 compares the experimental valence AFs so obtained with the PBE, HF, and HF + MP2 computed ones along the [110] and [111] crystallographic directions. The theoretical data include the damping factor $g(r,\sigma_{\mathrm{br}})$ [see discussion following Eq. (12)]. To show the effect of this correction, the uncorrected PBE data are reported as well: it is seen that, due to the high experimental resolution, the damping factor is still relatively unimportant in the region of interest (its value is 0.90 at 10 a.u. and 0.65 at 20 a.u.). The agreement between theory and experiment appears to be excellent and is slightly better with the more advanced level of theory. As

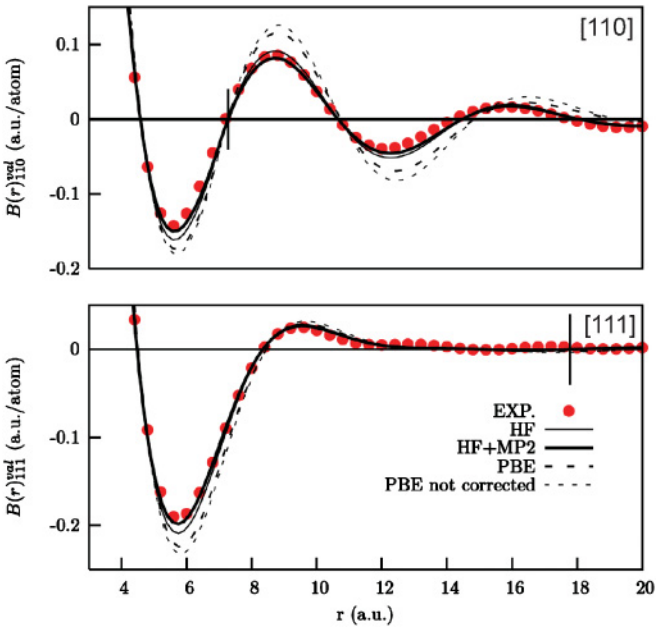

FIG. 4. (Color online) Valence AFs along the [110] and [111] directions computed at HF (thin solid lines), HF + MP2 (thick solid lines), and PBE (long-dashed lines) levels of theory. All these data are corrected for the finite experimental resolution; uncorrected PBE data are also reported (short-dashed lines). The *experimental* valence AFs [filled (red) circles] were obtained as described in the text. Vertical segments along the two zero lines mark the length of the respective shortest lattice vector R_L. These plots partially coincide with those reported in Ref. 18.

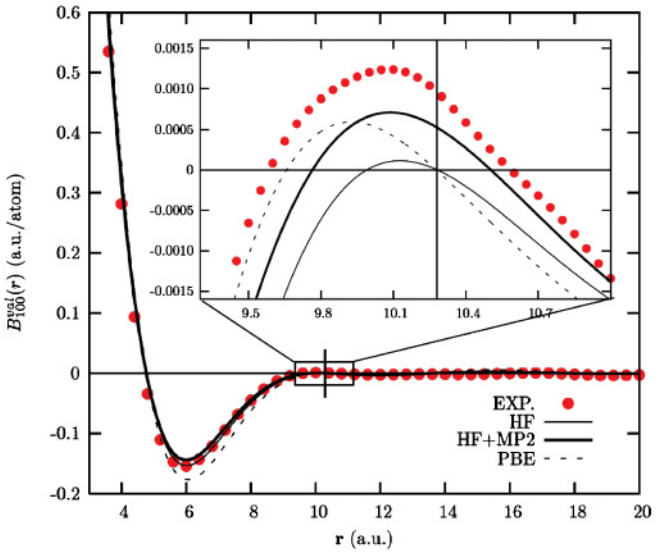

FIG. 5. (Color online) Theoretical and experimental valence AFs along the [100] crystallographic direction. Symbols as in Fig. 4. These plots partially coincide with those reported in Ref. 18.

already pointed out, also the valence AFs, computed from one-electron Hamiltonians, are expected to satisfy the nodal condition (13). The vertical segments mark the length of the shortest lattice vector R_L for the two directions where such zeros should occur. It is seen that the first nodal point along [111] is so far from the origin that the valence AF is there practically zero within the experimental errors. This is not true for the [110] AF, where the nodal condition is nicely satisfied by *all* theoretical curves and by the experimental one as well.

It was observed in Sec. IV that evidence of the inadequacy of the single-determinantal description of the wave function could come from the nonobservance of that property. As shown in Fig. 5, [100] is the only direction where a significant departure from that condition was observed: this is due to the fact that the corresponding R_L is still relatively short (10.28 a.u.) and that the AF in this case approaches the nodal point at a grazing angle, so that even a small correction may result in a notable departure from it. The inset in Fig. 5 shows the [100] AF data in a vicinity of the nodal point, at a very expanded scale. While the HF and PBE AFs are 0 at $r = R_L$, as expected, the intersection with the 0 axis occurs at $r/R_L =$ 1.02 for the HF + MP2 and 1.03 for the experimental AF.

D. Discussion

The comparison just performed between experimental and theoretical results concerning crystalline silicon confirms the generally recognized fact that DMs extracted from single-determinantal pseudo–wave functions provided by DFT calculations can very accurately reproduce ECD data, but perform rather poorly in reproducing quantities related to the distribution of electron momenta. HF-DMs behave oppositely, in a sense, by providing an unsatisfactory agreement with the experiment as concerns the ECD, while describing the EMD rather accurately, better than the DFT, in any case. The latter feature may be due to the fact that HF, at variance with the KS-DFT, describes *exactly* the Fermi hole, that is, the correlation among electrons with the same spin. It is not surprising, then, that a simple post-HF *ab initio* scheme like MP2 may provide results in very good agreement with experimental EMDs, while higher order corrections may be needed to obtain an accurate description of the calculated ECD. In particular, the extremely high resolution of the present experimental CPs has permitted us to clearly demonstrate the departure from the nodal condition of the [100] AF, which is reproduced rather faithfully by the post-HF scheme but cannot be accounted for by single-determinantal wave functions.

Definite discrepancies are left, however, between the HF + MP2 and the experimental EMD data. As just shown, they concern, in particular, the absolute value of the CP at low momenta (see Table II and Fig. 2) and the amount of departure from the nodal condition of the [100] AF (see Fig. 5). This disagreement may be attributed partly to experimental errors: the inadequacy of the impulse approximation or multiple scattering effects, only partly corrected for in the processing of the experimental data, have been invoked, for instance, to justify the systematic overestimation of theoretical with respect to experimental CPs at low momenta.[48] However, the discrepancy seems to exceed the estimated experimental uncertainties, so it can more likely be attributed to two kinds of deficiency of the present theoretical simulations: the level of the theoretical treatment and the neglect of nuclear motions.

As concerns the former aspect, the use of more flexible basis sets and the inclusion of higher orders than MP2 of the perturbative treatment might improve the agreement with the experiment. The fact must also be mentioned that in our Lagrangian scheme, orbital relaxation is not accounted for,[65] which may result in a small underestimation of the MP2 correction. Finally, as discussed in Sec. V B, the effect of both correlation and relativistic treatment of core electrons should be explicitly included.

Concerning the second aspect, we recall that all the present calculations refer to static nuclei with the lattice constant set at its experimental value at 300 K. This approximation does not affect our comparison with ECD data, because reference is made in Sec. V A to experimental data corrected for zero-point and thermal nuclear motion,[69] so the related disagreement must be traced back to the level of the "static" theoretical treatment. Instead, the EMD data analyzed in the following sections come from experiments carried out at room temperature, not corrected for nuclear motion; it would be desirable therefore to include these effects in the theoretical treatment. This is not an easy task, and to our knowledge, it has not received much attention in the literature so far. An interesting approach was proposed by Dugdale and Jarlborg for describing nuclear motion effects on the CP of alkali metals:[70] for this purpose they used a statistically averaged CP coming from a number of supercell calculations, each describing a thermally disordered distribution of the nuclear positions; electron correlation was accounted for by means of a modified Fermi distribution of level occupation. A different scheme was tried by Sternemann *et al.* for interpreting the change in the [110] CP of lithium when passing from 95 to 295 K;[71] the experimental results were in good agreement with LDA calculations, where an empirical pseudopotential was introduced, simulating on average thermal disorder; the experimental change in the lattice constant with temperature

was also accounted for. It can be noted incidentally that, according to the latter scheme, the nodal condition [Eq. (13)] remains satisfied with reference to the geometry adopted in each case. The case of silicon is so different from that of alkali metals that new techniques are required. However, the statistical approach just mentioned,[70] if suitably modified, can, in principle, be extended to nonconducting crystals.

VI. CONCLUSIONS

We have measured CPs of crystalline silicon and compared them to the predictions of *ab initio* simulations performed at different levels of theory. It has been shown that the manifold of KS orbitals, which provides an excellent description of the ECD, is inadequate for simulating properties related to the electron momentum distribution. In particular, as is the case for all schemes based on a single-determinantal approximation of the wave function, it cannot describe departures from the *nodal property* of the AF [Eq. (13)], which are instead observed experimentally. Such departures may be interpreted as fingerprint evidence of instantaneous Coulomb correlation effects: as a matter of fact, a simple post-HF (MP2) *ab initio* scheme newly implemented for periodic systems accounts for this effect nicely. More generally, the results obtained with the new scheme are in better agreement with the experimental CP data than those obtained with more conventional approaches.

Some discrepancies are left, however, which we have attributed to two main factors: partial inadequacy of the level of approximation adopted and neglect of nuclear motion effects. Work to improve the description of properties related to the DM of crystals is in progress in both directions. At the same time, new experimental CPs are presently planned for a number of systems, which will provide stringent tests of the accuracy of the calculations. These measurements will be characterized, on the one hand, by the fact that a rich set of directional CPs is considered, which permits, in principle, the full EMD to be reconstructed and, on the other hand, by the exploration of temperature effects.

We hope that the present study will provide a new stimulus for the production of very precise CPs for a variety of crystalline systems and for the refinement of existing theoretical tools for the description of their DM-related properties.

ACKNOWLEDGMENTS

The experiment at SPring-8 was performed with the approval of the Japan Synchrotron Radiation Research Institute (JASRI; Proposal No. 2009A2002). The authors are grateful to Denis Usvyat for useful discussions and suggestions.

*Corresponding author: alessandro.erba@unito.it
†Present address: Nanoscience Institute–CNR, Distretto Tecnologico ISUFI, Via per Arnesano, I-73100 Lecce, Italy

[1] A. Erba, C. Pisani, S. Casassa, L. Maschio, M. Schütz, and D. Usvyat, Phys. Rev. B **81**, 165108 (2010).
[2] A. J. Thakkar, Adv. Chem. Phys. **128**, 303 (2004).
[3] S. Ragot, J. Chem. Phys. **125**, 014106 (2006).
[4] J. R. Hart and A. J. Thakkar, Int. J. Quantum Chem. **102**, 673 (2005).
[5] Y. Sakurai, Y. Tanaka, A. Bansil, S. Kaprzyk, A. T. Stewart, Y. Nagashima, T. Hyodo, S. Nanao, H. Kawata, and N. Shiotani, Phys. Rev. Lett. **74**, 2252 (1995).
[6] C. Blaas, J. Redinger, S. Manninen, V. Honkimäki, K. Hämäläinen, and P. Suortti, Phys. Rev. Lett. **75**, 1984 (1995).
[7] M. Hakala, S. Huotari, K. Hämäläinen, S. Manninen, P. Wernet, A. Nilsson, and L. G. M. Pettersson, Phys. Rev. B **70**, 125413 (2004).
[8] M. Hakala, K. Nygård, S. Manninen, L. G. M. Pettersson, and K. Hämäläinen, Phys. Rev. B **73**, 035432 (2006).
[9] S. Sahoo, G. F. Gribakin, G. Shabbir Naz, J. Kohanoff, and D. Riley, Phys. Rev. E **77**, 046402 (2008).
[10] J. T. Okada, Y. Watanabe, S. Nanao, R. Tamura, S. Takeuchi, Y. Yokoyama, N. Hiraoka, M. Itou, and Y. Sakurai, Phys. Rev. B **68**, 132204 (2003).
[11] K. Nygård, M. Hakala, S. Manninen, K. Hämäläinen, M. Itou, A. Andrejczuk, and Y. Sakurai, Phys. Rev. B **73**, 024208 (2006).
[12] N. Hiraoka, T. Buslaps, V. Honkimäki, H. Minami, and H. Uwe, Phys. Rev. B **71**, 205106 (2005).
[13] P. E. Mijnarends, S. Kaprzyk, B. Barbiellini, Y. Li, J. F. Mitchell, P. A. Montano, and A. Bansil, Phys. Rev. B **75**, 014428 (2007).
[14] B. Barbiellini, C. Bellin, G. Loupias, T. Buslaps, and A. Shukla, Phys. Rev. B **79**, 155115 (2009).
[15] S. Ragot, J.-M. Gillet, and P. J. Becker, Phys. Rev. B **65**, 235115 (2002).
[16] C. Sternemann, S. Huotari, M. Hakala, M. Paulus, M. Volmer, C. Gutt, T. Buslaps, N. Hiraoka, D. D. Klug, K. Hämäläinen *et al.*, Phys. Rev. B **73**, 195104 (2006).
[17] A. Shukla, E. D. Isaacs, D. R. Hamann, and P. M. Platzman, Phys. Rev. B **64**, 052101 (2001).
[18] C. Pisani, M. Itou, Y. Sakurai, R. Yamaki, M. Ito, A. Erba, and L. Maschio, Phys. Chem. Chem. Phys. **13**, 933 (2011).
[19] C. Pisani, M. Busso, G. Capecchi, S. Casassa, R. Dovesi, L. Maschio, C. Zicovich-Wilson, and M. Schütz, J. Chem. Phys. **122**, 094113 (2005).
[20] C. Pisani, L. Maschio, S. Casassa, M. Halo, M. Schütz, and D. Usvyat, J. Comput. Chem. **29**, 2113 (2008).
[21] D. Usvyat, L. Maschio, F. R. Manby, S. Casassa, M. Schütz, and C. Pisani, Phys. Rev. B **76**, 075102 (2007).
[22] M. Schütz, D. Usvyat, M. Lorenz, C. Pisani, L. Maschio, S. Casassa, and M. Halo, in *Accurate Condensed Phase Quantum Chemistry*, edited by F. R. Manby (CRC Press, Boca Raton, FL, 2010), p. 29.
[23] P. Pulay, Chem. Phys. Lett. **100**, 151 (1983).
[24] R. Dovesi, V. R. Saunders, C. Roetti, R. Orlando, C. M. Zicovich-Wilson, F. Pascale, K. Doll, N. M. Harrison, B. Civalleri, I. J. Bush *et al.*, CRYSTAL09 *User's Manual* (University of Torino, Torino, 2006) [http://www.crystal.unito.it].
[25] M. Halo, S. Casassa, L. Maschio, and C. Pisani, Chem. Phys. Lett. **467**, 294 (2009).
[26] S. Casassa, M. Halo, and L. Maschio, J. Phys. Conf. Series **117**, 012007 (2008).

[27] M. Halo, S. Casassa, L. Maschio, and C. Pisani, Phys. Chem. Chem. Phys. **11**, 586 (2009).
[28] A. Erba, S. Casassa, L. Maschio, and C. Pisani, J. Phys. Chem. B **113**, 2347 (2009).
[29] A. Erba, S. Casassa, R. Dovesi, L. Maschio, and C. Pisani, J. Chem. Phys. **130**, 074505 (2009).
[30] C. Pisani, L. Maschio, S. Casassa, M. Halo, and A. Erba, Theor. Chem. Acc. **123**, 327 (2009).
[31] L. Maschio, D. Usvyat, M. Schütz, and B. Civalleri, J. Chem. Phys. **132**, 134706 (2010).
[32] L. Maschio, D. Usvyat, and B. Civalleri, Cryst. Eng. Commun. **12**, 2429 (2010).
[33] A. Erba, L. Maschio, S. Salustro, and S. Casassa, J. Chem. Phys. **134**, 074502 (2011).
[34] D. Usvyat, L. Maschio, C. Pisani, and M. Schütz, Z. Phys. Chem. **224**, 441 (2010).
[35] R. Martinez-Casado, G. Mallia, D. Usvyat, L. Maschio, S. Casassa, M. Schütz, and N. Harrison, J. Chem. Phys. **134**, 014706 (2011).
[36] M. Halo, S. Casassa, L. Maschio, C. Pisani, R. Dovesi, D. Ehinon, I. Baraille, M. Rérat, and D. Usvyat, Phys. Chem. Chem. Phys. **13**, 4434 (2011).
[37] C. Pisani, S. Casassa, and L. Maschio, Z. Phys. Chem. **220**, 913 (2006).
[38] J. C. Erskine and J. D. McGervey, Phys. Rev. **151**, 615 (1966).
[39] W. A. Reed and P. Eisenberger, Phys. Rev. B **6**, 4596 (1972).
[40] P. Pattison, N. K. Hansen, and J. R. Schneider, Chem. Phys. **59**, 231 (1981).
[41] N. Shiotani, N. Sakai, M. Ito, O. Mao, F. Itoh, H. Kawata, Y. Amemiya, and M. Ando, J. Phys. Condens. Matter **1**, 3270 (1989).
[42] Y. Kubo, Y. Sakurai, Y. Tanaka, T. Nakamura, H. Kawata, and N. Shiotani, J. Phys. Soc. Jpn. **66**, 2777 (1997).
[43] D. Stroud and H. Ehrenreich, Phys. Rev. **171**, 399 (1968).
[44] A. Seth and D. E. Ellis, J. Phys. C Solid State Phys. **10**, 181 (1977).
[45] F. M. Mueller, Phys. Rev. B **15**, 3039 (1977).
[46] H. Nara, K. Shindo, and T. Kobayashi, J. Phys. Soc. Jpn. **46**, 77 (1979).
[47] C. Pisani, R. Dovesi, and R. Orlando, Int. J. Quantum Chem. **42**, 5 (1992).
[48] B. Králik, P. Delaney, and S. G. Louie, Phys. Rev. Lett. **80**, 4253 (1998).
[49] M. Itou and Y. Sakurai, AIP Conf. Proc. **705**, 901 (2004).
[50] Y. Sakurai and M. Itou, J. Phys. Chem. Solids **65**, 2061 (2004).
[51] N. Sakai, J. Phys. Soc. Jpn. **56**, 2477 (1987).
[52] J. P. Perdew and A. Zunger, Phys. Rev. B **23**, 5048 (1981).
[53] J. P. Perdew, K. Burke, and M. Ernzerhof, Phys. Rev. Lett. **77**, 3865 (1996).
[54] A. D. Becke, J. Chem. Phys. **98**, 5648 (1993).
[55] G. H. Wannier, Phys. Rev. **52**, 191 (1937).
[56] C. M. Zicovich-Wilson, R. Dovesi, and V. R. Saunders, J. Chem. Phys. **115**, 9708 (2001).
[57] S. Casassa, C. M. Zicovich-Wilson, and C. Pisani, Theor. Chem. Acc. **116**, 726 (2006).
[58] P. Pulay and S. Saebø, Theor. Chim. Acta **69**, 357 (1986).
[59] L. Maschio and D. Usvyat, Phys. Rev. B **78**, 073102 (2008).
[60] C. Pisani, R. Dovesi, A. Erba, and P. Giannozzi, in *Modern Charge Density Analysis*, edited by C. Gatti and P. Macchi (Springer, Berlin, 2010).
[61] P. Giannozzi, S. Baroni, N. Bonini, M. Calandra, R. Car, C. Cavazzoni, D. Ceresoli, G. L. Chiarotti, M. Cococcioni, I. Dabo *et al.*, J. Phys. Condens. Matter **21**, 395502 (2009).
[62] E. A. Hylleraas, Z. Phys. **54**, 347 (1929).
[63] W. Kutzelnigg, Theor. Chim. Acta **68**, 445 (1985).
[64] T. Helgaker, P. Jørgensen, and J. Olsen, *Molecular Electronic Structure Theory* (John Wiley and Sons, Chichester, UK, 2000).
[65] D. Usvyat and M. Schütz, J. Phys. Conf. Ser. **117**, 012027 (2008).
[66] P. Pattison, W. Weyrich, and B. G. Williams, Solid State Commun. **21**, 967 (1977).
[67] A. J. Thakkar, A. M. Simas, and V. H. S. Jr., Chem. Phys. **63**, 175 (1981).
[68] M. Cooper, Adv. Phys. **20**, 453 (1971).
[69] Z. W. Lu, A. Zunger, and M. Deutsch, Phys. Rev. B **47**, 9385 (1993).
[70] S. B. Dugdale and T. Jarlborg, Solid State Commun. **105**, 283 (1998).
[71] C. Sternemann, G. Döring, C. Wittkop, W. Schülke, A. Shukla, T. Buslaps, and P. Suortti, J. Phys. Chem. Solids **61**, 379 (2000).